Norwegian Meteorological Institute

METreport

No. 14/2021
ISSN 2387-4201
Free

NGCD_rec, observational gridded datasets of monthly accumulated precipitation over Fennoscandia from 1901 to 2000

NGCD_rec, version 20.05

Cristian Lussana and Ole Einar Tveito

The Norwegian Meteorological Institute, Oslo, Norway

Francesco Isotta and Moritz Bandhauer

Federal Office of Meteorology and Climatology - METEOSWISS, Zurich, Switzerland

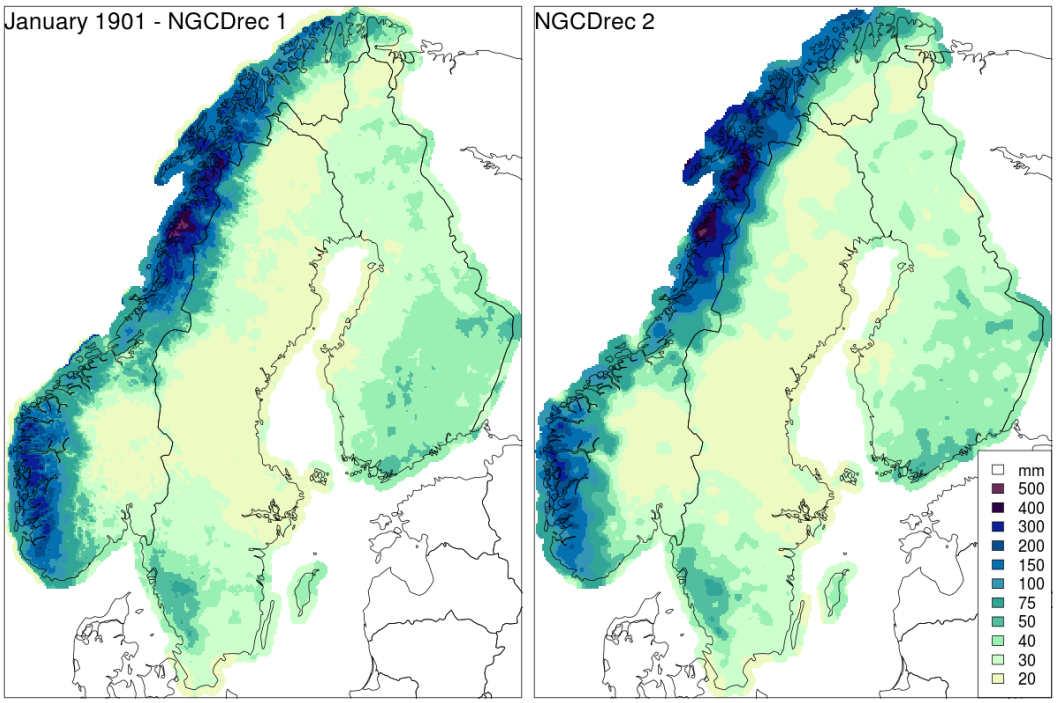

Norwegian Meteorological Institute

METreport

Title	Date
NGCD_rec, observational gridded datasets of monthly accumulated precipitation over Fennoscandia from 1901 to 2000.	March 3, 2022
Section	**Report no.**
Division for Climate Services	14/2021
Author(s)	**Classification**
Lussana C., Tveito O.E., Isotta F. and Bandhauer M.	● Free ○ Restricted

Abstract

The Nordic gridded climate dataset reconstruction (NGCD_rec) is a collection of observational gridded datasets of monthly accumulated precipitation covering Fennoscandia. The time period spanned is from 1901 to 2000 and the grid spacing is 5 km. The input data has been quality controlled but the time series have not been homogenized. The spatial analysis method employed is the reduced space optimal interpolation (RSOI). Two datasets (NGCD_rec 1 and 2) are provided for each period.

Keywords

observational gridded datasets, precipitation, climatology, RSOI

Disciplinary signature
Hans Olav Hygen

Responsible signature
Cecilie Stenersen

Norwegian Meteorological Institute
Org.no 971274042
post@met.no
www.met.no / www.yr.no

Oslo
P.O. Box 43, Blindern
0313 Oslo, Norway
T. +47 22 96 30 00

Bergen
Allégaten 70
5007 Bergen, Norway
T. +47 55 23 66 00

Tromsø
P.O. Box 6314, Langnes
9293 Tromsø, Norway
T. +47 77 62 13 00

Contents

1 Introduction

The number of observations of atmospheric variables near the Earth's surface has been constantly growing in recent years. For instance, in Norway the transition from manual to automatic weather stations allowed for an increase in the number of precipitation observations from 2010 onward (*Lussana et al.*, 2019), at the same time the sampling frequency of those measurements has increased up to one measure every few minutes. In the future, we will most likely have an unprecedented number of observed precipitation data available, collected by a large variety of data sources, ranging from satellites and weather radars to private weather stations (*Nipen et al.*, 2020; *Lussana et al.*, 2021), just to mention a few of them. A classical application in climatology is the reconstruction of past precipitation gridded fields over a domain based on an observational network of in-situ rain gauges. For this purpose, statistical methods are used to produce spatial predictions, or analysis, at grid points given the observed data. The resulting observational gridded datasets are widely used in climatology, but not only. For instance, in Norway, observational gridded datasets of daily precipitation totals, such as the seNorge datasets (*Lussana et al.*, 2019), are used as the atmospheric forcing for hydrological and snow modeling (*Skaugen and Mengistu*, 2016; *Saloranta*, 2016). However, there are periods in the past, such as the early part of the twentieth century, when the number of precipitation data available is limited, though it is still increasing thanks to numerous data recovery efforts. In this study we address a reconstruction of observational gridded datasets over periods where the observational network is varying significantly, specifically: can we "borrow strength" in the reconstruction over periods when the observational network is sparser from those periods when more observations are available? We investigate the reconstruction of gridded fields of monthly precipitation amounts over Fennoscandia, that is a region encompassing the Scandinavian peninsula and Finland, for the period of time between 1901 and year 2000.

The same issue has been addressed over the complex terrain of Switzerland by *Isotta et al.* (2019), in connection to the production of long-term consistent observational gridded datasets of monthly temperature and precipitation. The reconstruction method applied is the reduced space optimal interpolation (RSOI *Schiemann et al.*, 2010). RSOI is a method based on principal component analysis (PC *Wilks*, 2019) and it has been used to reconstruct gridded fields for time periods when the observational network was sparse by taking advantage of periods when the observational network was denser. The use of complete and homogenized time series ensures high-standard for long-term consistency

in the datasets over Switzerland, which span the period from 1864 to 2017. A similar work has been done in the past over Norway and the results are described by *Hisdal and Tveito* (1993). They applied the method of empirical orthogonal functions (EOF method), that is another name for PCA, to extend short runoff series based on the relation between short observed runoff series and a set of standardized regional EOFs (PCs).

The EOF method has also been applied to the spatial analysis of precipitation over Norway (*Tveito and Hisdal*, 1994) aiming at studying regional trends in annual and seasonal precipitation and runoff series.

The application of RSOI over Fennoscandia led to the production of the Nordic gridded climate dataset NGCD_rec, that is described in this report. NGCD_red is a long-term dataset of monthly precipitation totals that make available gridded fields for each month from January 1901 to December 2000. The Nordic countries covered by NGCD_rec are Finland, Norway and Sweden and the grid spacing of the final product has been set to 5 km in both zonal and meridional directions. The archive of monthly accumulated in-situ observations of precipitation considered is made of time series that have been quality controlled but that have not been homogenized yet. There is an ongoing effort in data collection, handling and homogenization of observational data aggregated on a monthly basis, that is known as the ClimNorm initiative and which is carried out thanks to the collaboration between the National Meteorological and Hydrological Services (NMHSs) of several Nordic countries. The current status of ClimNorm is documented in the report by *Tveito et al.* (2020). An updated version of NGCD_rec is planned once the ClimNorm initiative has provided homogenized monthly precipitation time series. The updates will cover also the years from 2001 to 2020. The NGCD_rec version documented in this report is ver. 20.05, which has been produced in 2020. In a sense, NGCD_rec ver. 20.05 represents a *feasibility study* in preparation of a future version that will be a long-term consistent observational gridded dataset, analogously to the above mentioned dataset produced by *Isotta et al.* (2019). In this version, we have preferred to favor the spatial detail represented in the long-term datasets rather than the robustness in the estimation. Specifically, a number of choices have been made to ensure consistent datasets, such as the use of a fixed set of stations within the time periods considered, however the optimization of RSOI has privileged the reconstruction of spatial details in the datasets. NGCD_rec is freely available to the public for use at `https://thredds.met.no/thredds/catalog/ngcd/NGCD_rec_version_20.05/catalog.html`. The dataset has an articulated structure and NGCD_rec is actually a collection of 16 gridded datasets. We have considered 8

different time periods that cover the longest interval from 1901 to 2000 in segments of ten years in ten years, such that we have: 1901-2000, 1910-2000, 1920-2000 and so on. The shortest time interval is 1971-2000. For each of the 8 time periods, we have decided to use two spatial analysis methods for reconstructing the high-resolution observational gridded dataset that is one of the steps in the production chain. This choice must be seen in the perspective that this version is still experimental in many ways, therefore we are testing different approaches. However, such a decision also represents an opportunity for those users who want to get an idea of the sensitivity of their application to slightly different input data.

The innovative parts of the presented research are only marginally in the RSOI method. Instead, they are mostly in the application of the method to a region where it has not been applied before and to an observational network that is varying significantly across the wide domain considered. What we have learned during our work and reported in this report may be of help to other groups who intend to apply RSOI outside the Alpine region, for instance. The application of RSOI based on two different statistical interpolation methods to obtain observational gridded datasets is also interesting, because it allows us to study the sensitivity of the methods to the input data. As for the method, we have applied a pre-processing data transformation based on Gaussian anamorphosis that is different from the square-root transformation applied by *Isotta et al.* (2019), which is the guide we have used to implement RSOI over Fennoscandia.

The document is organized as follows. In Sec. 2, the two data sources that are needed to apply RSOI are described. They are the archive of in-situ observations of monthly precipitation totals and the observational gridded dataset reconstructing the monthly precipitation fields in the data-rich time period. In Sec. 3, the RSOI method is described under a slightly different perspective than in the original article by *Schiemann et al.* (2010), though the final results are exactly the same. In this section we have used a point of view that is closer to inverse problem theory, as it has been formulated in the book by *Tarantola* (2005). The specific implementation of RSOI which has been used for the production of NGCD_rec ver. 20.05 is described in Sec. 4. In Sec. 5, NGCD_rec monthly precipitation fields are evaluated using cross-validation techniques. Furthermore, the evaluation of monthly fields is complemented by a validation of the mean annual precipitation fields. As an application of particular relevance, the extraction of temporal trends over the NGCD_rec grid is also presented in Sec. 5.3.

2 Data

2.1 The Nordic Gridded Climate Dataset (NGCD)

The gridded dataset produced to capture the spatial details of precipitation during the data-richest period is the Nordic Gridded Climate Dataset (NGCD). NGCD is a collection of two datasets of daily accumulated precipitation, where the definition of day used for the 24-hour aggregation is "from 06:00 UTC of the day in the timestamp, to 06:00 UTC of the previous day". The predicted fields are made available on a 1 km grid covering the time period from 1971 to 2020. The climatology of precipitation over Fennoscandia exhibits a seasonal behaviour. Stratiform precipitation occurs during wintertime, because of the frequent passages of low-pressure systems, and intense convective precipitation happens during summer. At the same time, the spatial variability of the precipitation field over Fennoscandia is remarkable, with the larger differences between the wetter Norwegian west coast and the dryer inland regions above the Arctic circle, where the annual total precipitation differs by almost one order of magnitude. NGCD allows for the study of the daily evolution of precipitation events and it is a product made available to all users interested in studying precipitation over Fennoscandia. The software used for the production of NGCD is freely available at `https://github.com/metno/NGCD`.

NGCD is produced by MET Norway, on behalf of the Copernicus Climate Change Services (C3S) aiming at monitoring European climate using surface observations `https://surfobs.climate.copernicus.eu`, and it is updated regularly every six months, in March and September. The version considered for the production of NGCD_rec is version 20.03 (March 2020), which is available at `https://thredds.met.no/thredds/catalog/ngcd/version_20.03/catalog.html`. The two datasets, NGCD-1 and NGCD-2, are based on the same input archive of in-situ observations but they have been obtained with two different spatial analysis methods. The observations used for Norway are extracted from the climate database of the Norwegian Meteorological Institute (accessible via `frost.met.no`). The observations used for Sweden, Finland are extracted from the European Climate Assessment & Dataset (ECA&D *Klein Tank et al.*, 2002). The input data coverage varies considerably throughout the period. The number of observations in 1971 was approximately 2300, it has increased just for a couple of years, then it has gradually decreased since the mid 1970s. The maximum number of observations was in autumn 1974, with data from 2518 stations. The lowest number of observations was at the

end of the period, with data from 1377 stations in December 2019. Despite the significant variations over time, the characteristics of the spatial distribution of the observational network do not change that much in time and they are quite similar to those of the networks used for NGCD_rec. The density of observations is higher in the southern part of the domain and near the largest cities. The observational network becomes more and more scattered the more we move north.

In the case of NGCD-1, the gridded precipitation is achieved by a Triangular Irregular Network (TIN) approach, also known as Delaunay triangulation. The method is based on triangulation of both observed precipitation and the elevation at the observing stations. The difference between the triangulated elevation surface and the 1 by 1 km^2 elevation model is used to adjust the triangulated precipitation surface to the correct elevation level. The Global 30 Arc-Second Elevation Data Set (GTOPO30 *Gesch et al.*, 1999), a global raster Digital Elevation Model (DEM) with a horizontal grid spacing of 30 arc seconds (approximately 1 kilometer) developed by U.S. Geological Survey (USGS) is used to create the required elevation fields. The method is described more in detail in *Tveito et al.* (2005) and it has been applied to obtain the first version of the seNorge observational gridded dataset (*Mohr*, 2008, 2009), that is a national gridded dataset used in Norway (*Saloranta*, 2012; *Skaugen and Onof*, 2014; *Gisnås et al.*, 2016). NGCD-2 precipitation fields are created by a procedure based on a multi-scale Optimal Interpolation (OI *Gandin and Hardin*, 1965) applied sequentially over a decreasing sequence of length scales. The implementation of the method resembles successive correction methods (*Uboldi and Buzzi*, 1994) and it has been described in detail by *Lussana et al.* (2018a). NGCD-2 is based on the method used to implement seNorge version 2. The two spatial analysis methods used for NGCD-1 and NGCD-2 have been compared over Norway and the comparison between seNorge version 1.1 (NGCD-1 method) and version 2 (NGCD-2 method) is described in the paper by *Lussana et al.* (2018a). The indirect evaluation of the precipitation fields through the comparison to hydrological observations show that seNorge1.1 has higher annual total precipitation than the water losses for most catchments, while seNorge2 underestimates the input term in the water balance. In the same publication, seNorge2 daily precipitation has been compared to E-OBS (*Cornes et al.*, 2018), which is an observational dataset covering Europe, and the two datasets show similar results. In the mountains, where the observational network is sparser and most of the stations lie on the valley floors (*Lussana et al.*, 2019), seNorge2 underestimates precipitation if compared to E-OBS. In conclusion, if compared to hydrological observations and to other datasets,

seNorge2 provides less accurate (i.e., higher bias) but more precise (i.e., lower spread) estimates of the annual averaged precipitation than seNorge1.1.

NGCD datasets have been post-processed before using them within the NGCD_rec production chain. NGCD daily fields have been summed up to obtain monthly totals, then we have upscaled the 1 km precipitation fields onto a grid with spacing of 5 km. The regridding from the finer to the coarser grid is made by spatial averaging of all grid points of the fine grid within the boxes of the coarser grid.

It is worth noting that considering any month in the calibration period, NGCD provides a better description of precipitation, as we used the largest number of observations available for each day of that month. However, for all those applications that require time coherence, such as for example the calculation of time trends, NGCD_rec represents a dataset more suitable for the purpose since a fixed station dataset is used and this also applies to the calibration period.

2.2 The archive of in-situ observations of monthly precipitation

The archive of in-situ observations is the dataset of long-term high-quality time series of observations of monthly precipitation totals measured by climatological stations provided by the National Meteorological and Hydrological Services (NMHS) of Finland, Norway and Sweden. Because those NMHSs are also providing data to ECA&D, there are overlaps between the time series included in both datasets. It is worth remarking once again that the time series considered in the production of NGCD_rec have not been homogenized.

For being used in the production of NGCD_rec, a time series needs to be complete, gaps in the data are not allowed. The longer the period considered, the less are the stations satisfying this requirement. The time intervals we have considered are shown in Figs. 1-2 and they are: 1901-2000, 1911-2000, 1921-2000, 1931-2000, 1941-2000, 1951-2000, 1961-2000 and 1971-2000. For each of these time intervals a gridded dataset with the reconstructed fields has been created and the collection of all these datasets constitute NGCD_rec. The datasets are listed in Tab. 1, together with the number of observations available. The station density determines locally the quality of the reconstruction and for this reason we have decided to include in Tab. 1 three descriptive parameters related to this quantity, namely: The second and the third columns report the number of stations in data-dense and -sparse regions, the fourth column is the distance D between a station and its closest third station. The station density is quantified through the cross-validation integral

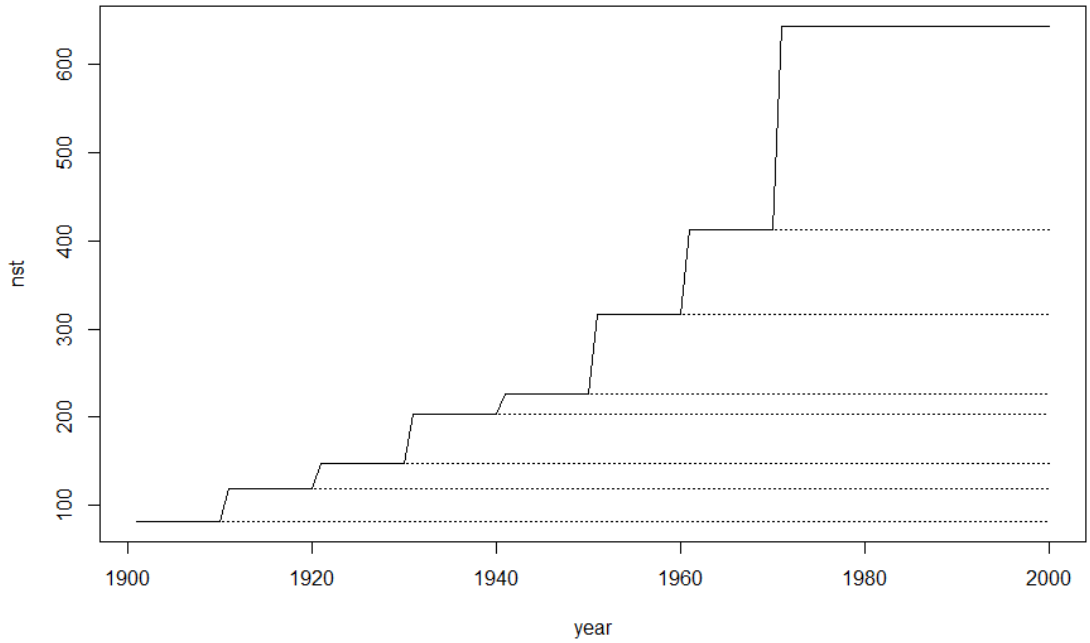

Figure 1: Number of time series of in-situ observations of monthly precipitation totals used in the reconstructions of the NGCD_rec datasets listed in Tab. 1

.

data influence (CV-IDI *Uboldi et al.*, 2008), which is equal to 1 for stations located in data-rich areas, while stations in data-void regions are assigned a CV-IDI of 0. The reference horizontal (radial) length scale used in the CV-IDI calculations has been set for all datasets to 55 km, that is the mean value between the smaller (37 km) and the larger (73 km) values of D. As done by e.g. *Cardinali et al.* (2004); *Lussana et al.* (2018b), stations are assumed to lie in data-sparse regions when CV-IDI is less than 0.45, while they are in data-dense regions if CV-IDI is greater than 0.85. Figure 1 shows the availability of series for ten years in ten years. Figure 2 shows the spatial distribution of these series. The longer time period considered is from 1901 to 2000, in this period we are using less than 5 stations in Finland and around 20 in Sweden. Then, the number of time series available is slowly increasing and for the period 1931-2000 it is 201, then for 1961-2000 is 373. The most recent period considered overlaps with the period when NGCD is available and it is 1971-2000, when 596 time series have been used. As can be seen from Tab. 1, for the period 1901-2000 we are using only 13% of the stations available for 1971-2000. The fraction of the number of stations in data-dense regions is even less, in fact for 1901-2000 there

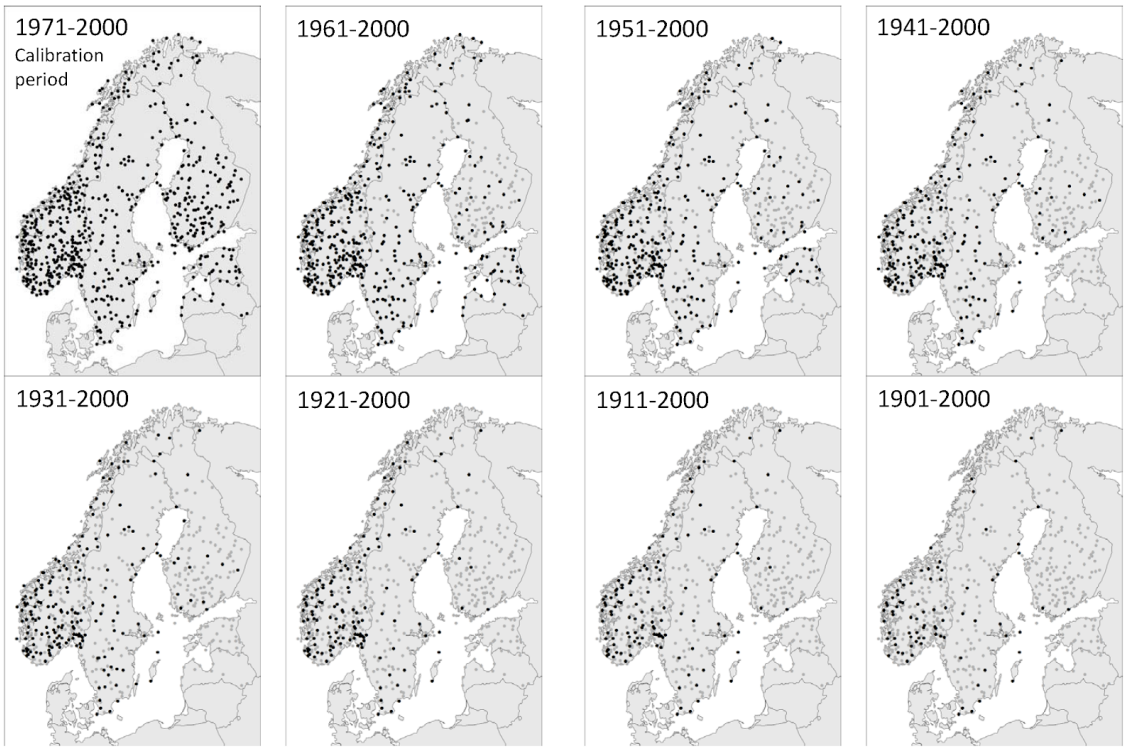

Figure 2: Spatial distribution of the series applied for the construction of the NGCD_rec time slices listed in Tab. 1. Black dots represent series with complete records. Grey dots represent incomplete series not applied for reconstruction.

are 7% of the stations available in data-dense regions for 1971-2000.

For all periods, the observational network is unevenly distributed over Fennoscandia and clusters of stations can be identified near the big cities, especially in Southern Norway. The effects of this inhomogeneous spatial distribution can be seen in Tab. 1. For instance, if we compare the observational network in 1921-2000 to that available in 1931-2000, there is an increase in the number of stations (1931-2000 has +40% of the stations available in 1921-2000), which corresponds to a better coverage of the domain because in 1931-2000 there are stations in previously data-void regions. However, the distance D does not decrease, on the contrary it increases by only 1 km, because the increase in the number of stations does not correspond to a significant increase in the station density. For instance, if we consider 1921-2000 the fraction of stations in data-dense regions is 64%, which is comparable to 68% in 1931-2000.

The station density quantified through the CV-IDI is the horizontal density of observations, since elevation is not considered. The spatial distribution of observations in

Norway, which is the region where the terrain is more mountainous, is extensively discussed by *Lussana et al.* (2019). The observational network is unevenly distributed along the range of altitudes as can be seen in Fig.1 of the paper by *Lussana et al.* (2019). Given the difficulty in operating stations in such an environment, the upper half of the altitude range is heavily lacking in measuring stations. Over the westernmost part of Norway, for instance, the highest peaks exceed 2000 meters, but unfortunately only very few stations reach these altitudes. Most of the stations are located at the bottom of the valley, at altitudes often below 1000 meters. A very similar situation occurs on the northern border between Sweden and Norway, where the highest mountains in Sweden are located, such as the Kebnekaise massif. This range of the Scandinavian mountains reaches values just over 2000 meters, while the stations at the highest altitudes are located between 500 and 800 meters.

3 Reduced space optimal interpolation (RSOI) method

The objective is to create a gridded dataset for a meteorological quantity Q covering a time period T^r (reconstruction time period) based on observed data from a network of p stations, constantly available over T^r.

Suppose that a gridded dataset for the same variable is also available over a time period T^c (calibration time period), where T^c is shorter than T^r. The gridded dataset represents our best knowledge of Q over a spatial domain and it may have been obtained from an observational network that is different from the one available in T^r. The idea is to extract from the gridded dataset information on the climatology of Q and use this information to increase the quality of the reconstructed dataset over T^r. A possible way to extract climatological information is to perform a principal component analysis (PC). We extract the first l components of the gridded dataset over T^c. They are stored as columns in the m by l matrix $\mathbf{E}$. The PC-scores are also stored for each observation time included in T^c as the l vector $\mathbf{a}^c(t)$. Note that we assume all vectors to be column vectors. PC can be used to represent a "smoothed" version of each gridded field in T^c as:

$$\mathbf{x}(t) = \mathbf{E}\,\mathbf{a}^c(t)\ , t \in T^c \tag{1}$$

$\mathbf{x}(t)$ is a m-vector representing a gridded field at time t.

The final product sought is a gridded dataset over T^r where the field at time t is written as:

$$\mathbf{x}^{\mathrm{a}}(t) = \mathbf{E}\,\mathbf{a}(t)\,, t \in T^r \tag{2}$$

where the l-vector of coefficients $\mathbf{a}(t)$ has been chosen as a function of the observations, in some optimal way. The p-vector of the observations is indicated as $\mathbf{y}^{\mathrm{o}}(t)$. In this sense, $\mathbf{x}^{\mathrm{a}}(t)$ is our best estimate of the field based on the p observed data and "borrowing strength" from the gridded dataset used for calibration, through the use of $\mathbf{E}$. We assume the PC-loadings $\mathbf{E}$, derived over T^c, are a useful orthonormal basis also over T^r.

In the remaining of this section, the calculation of $\mathbf{a}(t)$ in Eq. (2) is described. The procedure described is valid for an arbitrary value of t and it has to be applied to all $t \in T^r$. For the sake of brevity, all quantities from now on refer to this t and we drop the time index.

We want to obtain an estimator of the unknown true value of $\mathbf{a}$, defined as the l-vector $\mathbf{a}^{\mathrm{t}}$, which are the PC-scores we would have if we had all the knowledge on T^r that we had for T^c.

The relation between $\mathbf{y}^{\mathrm{o}}$ and $\mathbf{a}^{\mathrm{t}}$ can be written as:

$$\mathbf{y}^{\mathrm{o}} = \mathbf{H}^{\mathrm{o}}\mathbf{E}\,\mathbf{a}^{\mathrm{t}} + \varepsilon^{\mathrm{o}} = \mathbf{H}\,\mathbf{a}^{\mathrm{t}} + \varepsilon^{\mathrm{o}} \tag{3}$$

$\mathbf{H}$ is the observation operator (or forward model), that is a function mapping $\mathbb{R}^l$ into $\mathbb{R}^p$. In our case, $\mathbf{H}$ is a matrix multiplication and it is equivalent to extracting the PC-loadings values at the p station locations. ε^o is the p-vector observation error and it is assumed to be a multivariate normal (MVN or N):

$$\varepsilon^o \sim N(\mathbf{0}, \mathbf{R}) \tag{4}$$

$\mathbf{R}$ is the observation error covariance matrix and it is defined as $\langle \varepsilon^o \varepsilon^{o\mathrm{T}} \rangle$ ($\langle \ldots \rangle$ is the expected value over an ensemble of realizations). Since in the calibration period T^c the true values of the $\mathbf{a}$ coefficients are known, as they are the PC-scores $\mathbf{a}^{\mathrm{c}}_t$ in Eq. (1), it is possible to estimate $\mathbf{R}$ as:

$$\mathbf{R} = \left\langle \left(\mathbf{y}^{\mathrm{o}} - \mathbf{H}\mathbf{a}^{\mathrm{c}}\right)\left(\mathbf{y}^{\mathrm{o}} - \mathbf{H}\mathbf{a}^{\mathrm{c}}\right)^{\mathrm{T}} \right\rangle_{T^c} \tag{5}$$

where the expectation operator is approximated with $\langle \ldots \rangle_{T^c}$, which is the average over the realization in T^c.

We consider an a-priori information on $\mathbf{a}$, that is stored as the vector of background values $\mathbf{a}^{\mathrm{b}}$. The relation between $\mathbf{a}^{\mathrm{b}}$ and $\mathbf{a}^{\mathrm{t}}$ is:

$$\mathbf{a}^{\mathrm{b}} = \mathbf{a}^{\mathrm{t}} + \eta^{b} \tag{6}$$

η^{b} is the l-vector of the background error and it is assumed to be a multivariate Gaussian:

$$\eta^{b} \sim N(\mathbf{0}, \mathbf{C}) \tag{7}$$

The l background values are always set to 0, such that $\mathbf{a}^{\mathrm{b}} = \mathbf{0}$. The background error covariance matrix (l x l) $\mathbf{C}$ is fixed in time, it is diagonal and its components are the eigenvalues associated to the PC-loadings (i.e., the eigenvectors of a covariance matrix). An advantage of working with PC is that this justifies the use of a diagonal $\mathbf{C}$. The larger the eigenvalue, the less precise is our guess of $\mathbf{a}^{\mathrm{t}}$ by the background or, in other words, the more likely would be the corresponding component of $\mathbf{a}^{\mathrm{a}}$ to deviate from 0. From another point of view again, small eigenvalues dump the importance of the corresponding PC-loadings because the $\mathbf{a}^{\mathrm{a}}$ component would stay close to zero.

From linear filtering theory (*Jazwinski*, 2007) and given the assumptions above, the combination of observation and background information yields the analysis $\mathbf{a}^{\mathrm{a}}$, that is the best (i.e., minimum analysis error variance), linear, unbiased estimate of the true state. The analysis can be written as:

$$\mathbf{a}^{\mathrm{a}} = \mathbf{a}^{\mathrm{b}} + \mathbf{K}\left(\mathbf{y}^{\mathrm{o}} - \mathbf{H}\mathbf{a}^{\mathrm{b}}\right) = \mathbf{K}\mathbf{y}^{\mathrm{o}} \tag{8}$$

The final dataset can be obtained by using the value of $\mathbf{a}^{\mathrm{a}}$ in Eq. (2), for different values of t. It is worth remarking that we search the best value of $\mathbf{a}$ within the sub-space of values spanned by the linear combinations of the observations $\mathbf{y}^{\mathrm{o}}$. In inverse problem theory (*Tarantola*, 2005), Eq. (8) is obtained as the result of least squares techniques. In data assimilation (*Carrassi et al.*, 2018), Eq. (8) is referred to as the analysis step of sequential Kalman filters or Optimal Interpolation. The gain matrix $\mathbf{K}$ can be obtained by means of one of the two expressions:

$$\mathbf{K} = \mathbf{C}\mathbf{H}^{\mathrm{T}}\left(\mathbf{H}\mathbf{C}\mathbf{H}^{\mathrm{T}} + \mathbf{R}\right)^{-1} \tag{9}$$

$$\mathbf{K} = \left(\mathbf{H}^{\mathrm{T}}\mathbf{R}^{-1}\mathbf{H} + \mathbf{C}^{-1}\right)^{-1}\mathbf{H}^{\mathrm{T}}\mathbf{R}^{-1} \tag{10}$$

which are equivalent, as can be shown using the Sherman-Morrison-Woodbury formula (*Hager*, 1989), taking into account that $\mathbf{C}$ is diagonal.

4 Implementation of RSOI

The two data sources used, NGCD and the archive of monthly precipitation totals, have been described in Sec. 2. The RSOI method has been described in Sec. 3. In this section, the implementation choices that have been made to obtain NGCD_rec are described.

In the paper by *Isotta et al.* (2019), they recommend transforming the precipitation data before applying RSOI, in order to reduce the skewness of the distribution of values. They found a square-root transformation to be suitable for their application. In this work, the monthly totals have been transformed from their original distribution of values into a more symmetric, bell-shaped distribution through a Gaussian anamorphosis, similarly to what done by *Lussana et al.* (2021). We assume the monthly totals follow a gamma distribution and constant values of the gamma parameters' shape and rate are used in the transformation over the whole domain. We have used the 5 km upscaled NGCD to estimate the constant shape and rate, which are applied to all datasets listed in Tab. 1. Precisely, NGCD-1 is used for obtaining shape and rate for NGCD_rec-1 and NGCD-2 for NGCD_rec-2 datasets. The values of shape and rate are the maximum likelihood estimators calculated iteratively by means of the Newton–Raphson method as described by *Wilks* (2019), Sect. 4.6.2. A schematic description of the whole process can be found in Fig. 8 of *Lussana et al.* (2021). For NGCD_rec-1 the shape is equal to 1.637 and the rate is equal to 0.019. For NGCD_rec-2 the shape is equal to 1.397 and the rate is equal to 0.021. After the application of RSOI, the reconstructed fields are back-transformed into precipitation values by means of the inverse transformation, that is from standard normal to gamma distributed values. The benefits of the Gaussian anamorphosis compared to the square-root transformation are practically nil, we have compared the two transformations and the aggregated results are identical. We have decided to use the Gaussian anamorphosis because we found there was a slight improvement for some isolated stations and the cross-validation results were better for NGCD_rec-1 1901-2000 and almost identical in the other cases.

The most important RSOI parameter to set is the number of PC components l. We have chosen to use $l = 40$ for all NGCD_rec datasets listed in Tab. 1. If we consider NGCD_rec-1/2 1971-2000, the cumulative explained variance fraction with $l = 40$ is greater than 90%. We have made leave-one-out cross-validation experiments, of the type described in Sec. 5.1, with several values of l, specifically we have used: 5, 20, 30, 40 and 50. In Figure 3, the mean-squared error skill score (MSESS *Wilks*, 2019; *Isotta et al.*,

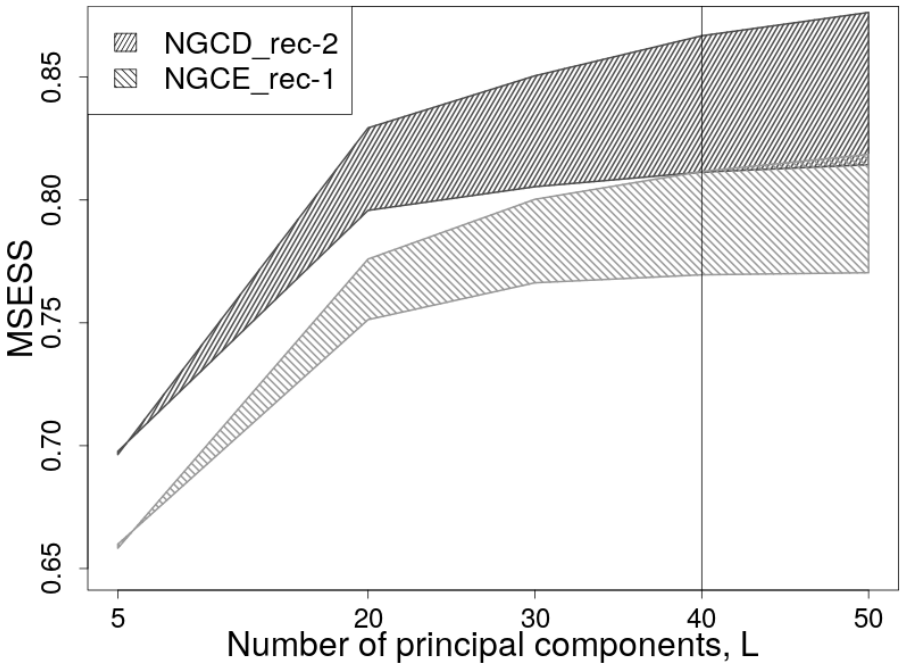

Figure 3: MSESS as a function of the number of principal components retained in the reconstruction l. The two polygons refer to NGCD_rec-1 and 2, as reported in the legend. The area within each polygon is delimited by the MSESSs of the 1901-2000 (bottom line) and the 1971-2000 (top line) datasets. The vertical black line marks our choice on $l = 40$.

2019) is shown as a function of l for NGCD_rec-1 and 2. The MSESS is equal to 1 when the agreement is optimal, while it is close to zero or negative when the mean squared deviation between predicted and observed values is equal to or larger than the variance of the time series. First, the MSESS has been computed on a station-by-station basis to quantify the agreement between predicted and observed values. For each time period, the values considered in the calculation of MSESS cover the whole period, therefore for datasets on 1901-2000 we have used 100 years of data, while only 30 years have been used for datasets over 1971-2000. The polygons shown in Fig. 3 summarize the MSESS statistics for NGCD_rec-1 and 2 and the area of the polygons are bounded by the MSESS for 1971-2000 (top lines) and for 1901-2000 (bottom lines). The trend of the two polygons is similar, though NGCD_rec-2 shows better MSESS values. The curves begin to flatten around the value of $l = 30$ and the MSESS variations between $l = 50$ and $l = 40$ are less than 1% of the MSESS for $l = 50$. Therefore, we have concluded that continuing to add components in addition to 40 does not add significant benefits and this prompted us to choose $l = 40$.

5 Results

5.1 Evaluation

The evaluation presented is based on the comparison between observations and predictions obtained through leave-one-out cross-validation, therefore each prediction is independent from the corresponding observation. We have considered several evaluation scores, the one that is used more often is the MSESS, which has been introduced in Sec. 4. Furthermore, as in Sec. 4, the station density is quantified through CV-IDI.

The two main factors determining the quality of the reconstructed fields are the seasonality of precipitation and the station density. In Tab. 2 the MSESS statistics are reported for each dataset. NGCD_rec-2 scores better than NGCD_rec-1 and, as we will see, this happens for all the scores presented in the following. In the table, the scores are divided by season and the results have also been disaggregated into data-sparse and data-dense regions, such that it is possible to have an idea of the variability of the results. In general, the more stations are used in the reconstruction, the higher is the corresponding MSESS and for this reason the datasets for 1971-2000 show better results than those for 1901-2000. NGCD_rec reaches its better performances during autumn and winter, when precipitation is dominated by events with the largest spatial scales associated with stratiform precipitation. In summer, the reconstruction scores are worse than in the other months, probably because a larger proportion of convective episodes occur and a denser network would be needed to improve the performances. The seasonality determines the MSESS average value, for instance, summer presents scores that differ from the higher winter values by approximately 0.1 units. Then, within each season it is mainly the local station density influencing the quality of the reconstruction, as can be seen from the spread represented by the range of values in data-dense and data-sparse regions. However, NGCD_rec-1 1971-2000 makes an exception in the spring and summer seasons, where the scores do not depend on the station density but probably they are more influenced by the characteristics of the statistical interpolation method applied to NGCD-1, as explained in the following.

The comparison between predicted and observed values for NGCD_rec-1 1971-2000 and NGCD_rec-2 1971-2000 are shown in the scatterplot of Fig. 4. The time period considered is the entire 1971-2000 period. NGCD_rec-1 1971-2000 tends to overestimate precipitation, the regression line has a slope of 1.11 (i.e. predicted = 1.11 * observed).

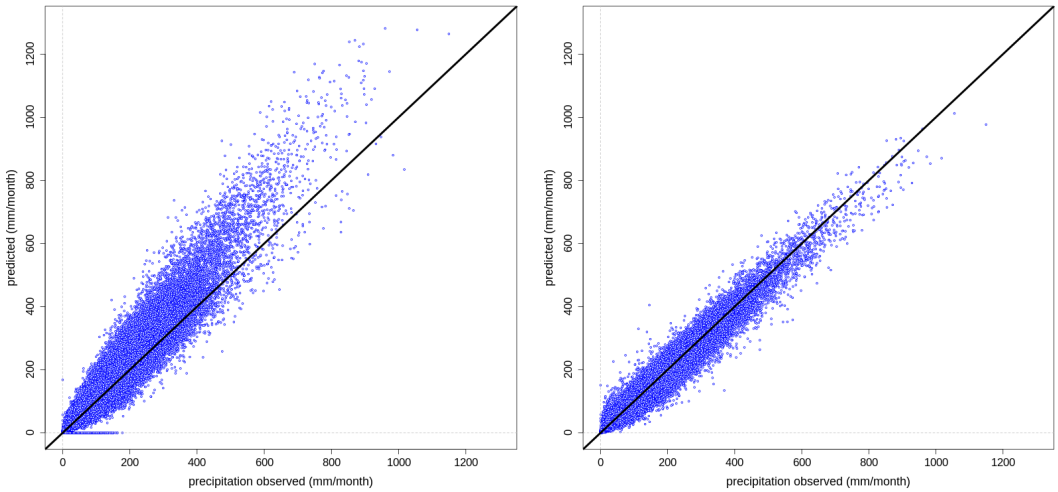

Figure 4: Monthly precipitation values: predicted versus observed for NGCD_rec-1 1971-2000 (left) and NGCD_rec-2 1971-2000 (right). The predicted values have been obtained through cross-validation. The black line is the 1:1 line.

A few points along the coast report no precipitation for the entire period, this is an issue of the spatial interpolation method based on TIN. The regression line computed for NGCD_rec-2 1971-2000 has a slope of 0.96. NGCD_rec-2 1971-2000 is more likely to underestimate precipitation and the predictions are more precise than those of NGCD_rec-1 1971-2000, as can be seen by the smaller dispersion of the predicted values around the ideal 1:1 line. The scatterplots referring to the other time periods, from 1961-2000 to 1901-2000, have been produced but they are not shown here because they are all similar to Fig. 4. For instance, in the case of NGCD_rec-1/2 1901-2000 the angular coefficients are: 1.06 for NGCD_rec-1 and 0.97 for NGCD_rec-2.

In Figure 5, MSESS is shown station by station for NGCD_rec-1/2 1971-2000. Figs. 6-7 refer to NGCD_rec-1/2 1941-2000 and NGCD_rec-1/2 1901-2000, respectively, and their layouts are the same as that of Fig. 5. The insets at the top left corner of each map show the MSESS as a function of the station density. In general, the denser the observational network, the better the reconstruction. However, in Fig. 5, the relationship between station density and quality of the reconstruction is less evident for NGCD_rec-1 1971-2000. For this dataset, stations on the western coast of Norway, which are located in a data-dense region, do actually have quite low MSESS values. This situation has also an impact on the scores reported in Tab. 2, as mentioned above.

The time series shown in Fig. 8 help to explain the situation. The location of the

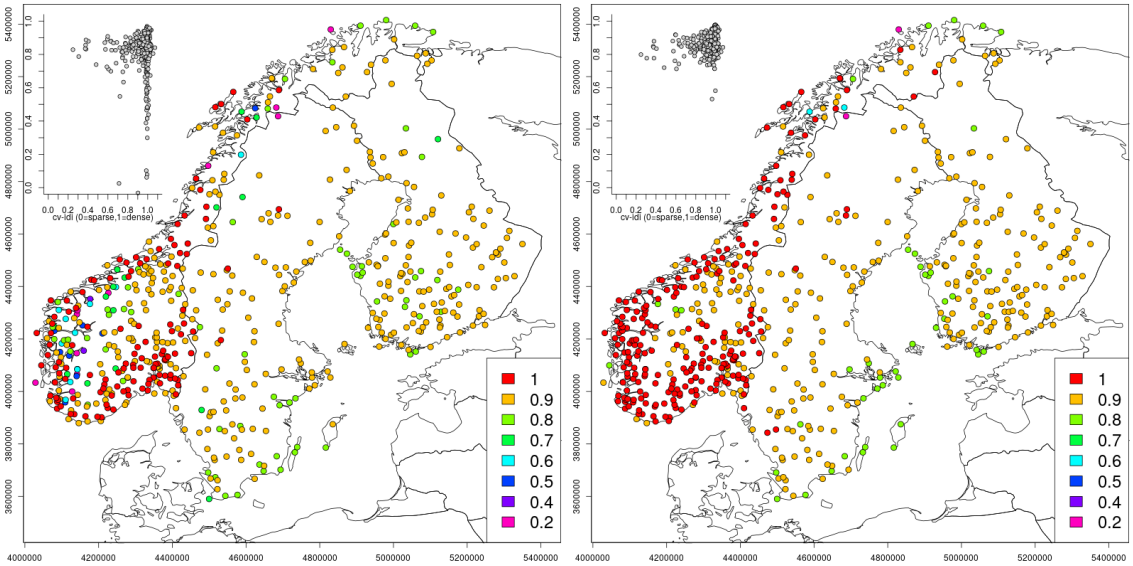

Figure 5: MSESS statistics for NGCD_rec-1 1971-2000 (left) and NGCD_rec-2 1971-2000 (right). The dots represent the stations used and the colours the MSESS values for each station. The spatial reference is ETRS89 / ETRS-LAEA https://spatialreference.org/ref/epsg/etrs89-etrs-laea/ the units of the spatial coordinates are meters. The box at the upper-left corner of each figure shows the MSESS for each station as a function of the cross-validation integral data influence (CV-IDI, Sec. 2.2; CV-IDI=1 data-rich area; CV-IDI=0 data-void area).

station considered is shown in the left panel, while in the right panel the time series of the observed and (leave-one-out) predicted values are shown. The MSESS value for NGCD_rec-1 1971-2000 is 0.08, while the MSESS for NGCD_rec-2 1971-2000 is 0.97. The correlation between the predicted and observed time series is equal to 0.98, which is a remarkably high value, for both versions of NGCD_rec. The weak point of NGCD_rec-1 is that it overestimates significantly the peaks of precipitation during winter and autumn. The root mean square deviation between observations and predictions at this location is 117 mm/month for NGCD_rec-1 and 23 mm/month for NGCD_rec-2 and the root mean squared factor (*Golding*, 1998) is 1.78 for NGCD_rec-1 and 1.26 for NGCD_rec-2. The reason behind the overestimation is in the method applied for NGCD-1, which has been introduced in Sec. 2.1, and that is trying to compensate for the uneven distribution of stations across the range of altitudes by systematically increasing the amount of predicted precipitation with the elevation. In the west coast of Norway, the stations are often located on valley floors, as discussed in Sec. 2.2, which are surrounded by steep slopes and

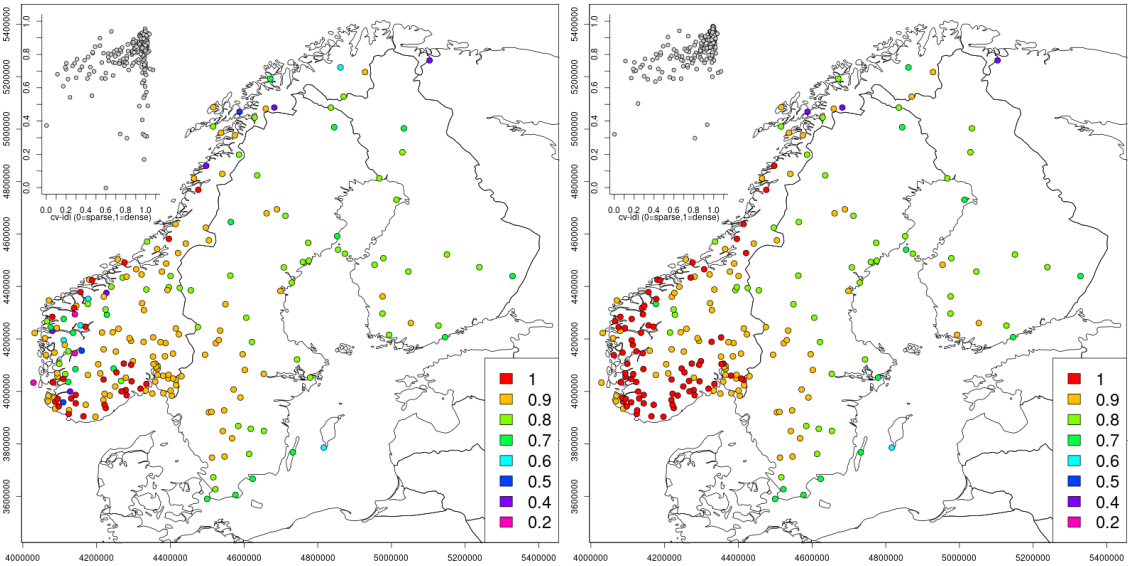

Figure 6: MSESS statistics as in Fig. 5, but for NGCD_rec-1 1941-2000 (left) and NGCD_rec-2 1941-2000.

mountain tops. The precipitation value reconstructed by NGCD-1 is designed to be more representative of the points at the average elevation of a 5 by 5 km^2 cell than the measurements on the valley floor and this explains the low score when the number of stations in these areas of complex terrain increases.

Another special case is presented in Fig. 9, the station considered is again in a region of complex terrain along the border between Sweden and Finland, where the mountain tops reach elevations just over 2000 meters, while the sparse stations are located on the valley floors, about 1000 meters below. At this location, both NGCD_rec versions are not able to reconstruct the observed values in a satisfying way. In fact, the MSESS has negative values for both and the correlations are: 0.76 for NGCD_rec-1 and 0.61 for NGCD_rec-2.

Apart from the special cases discussed above, the quality of the reconstruction is rather high, according to the MSESS shown in Fig. 5, also for stations in very sparse regions. For instance, for NGCD_rec-2, where CV-IDI is around 0.4, the MSESS still remains greater than 0.7 and close to 0.8. The MSESS of NGCD_rec-1 and NGCD_rec-2 are similar over Sweden and Finland and often greater than 0.7. Over Norway, there are differences between the two types of NGCD_rec, as discussed above. The comparison of Figs. 6- 7 against Fig. 5 once again shows the difference between the number and the spatial distribution of the stations used for the different periods. In particular, very

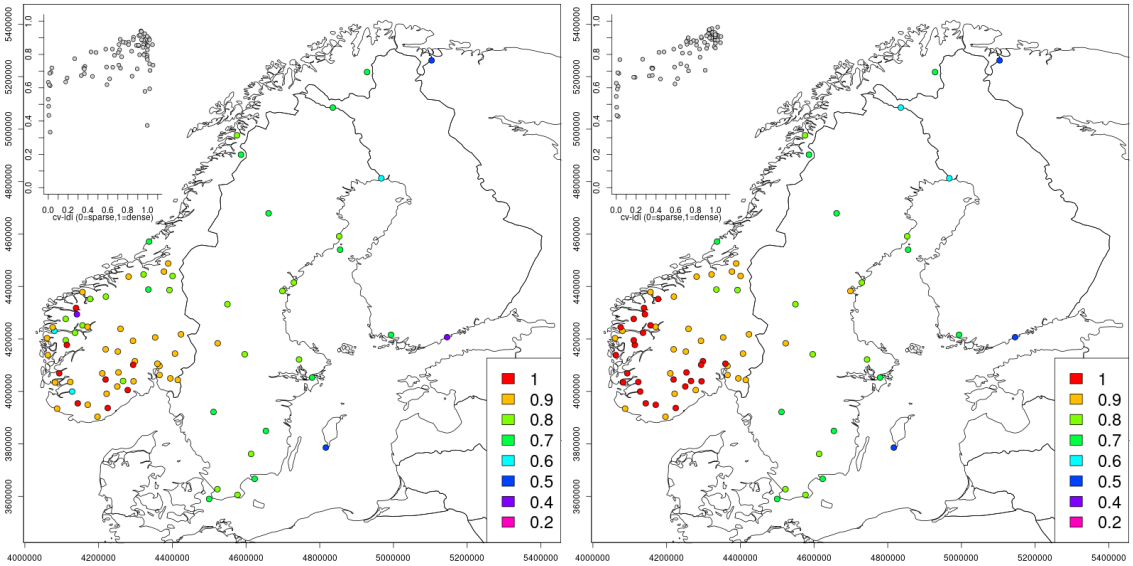

Figure 7: MSESS statistics as in Fig. 5, but for NGCD_rec-1 1901-2000 (left) and NGCD_rec-2 1901-2000.

few stations over Finland and Sweden have been used for NGCD_rec-1/2 1901-2000. For this reason, a certain caution is advised in using NGCD_rec-1/2 1901-2000 for these countries. Nevertheless, the evaluation based on MSESS shows that the quality of the reconstruction is still acceptable, especially over Sweden where the MSESS is almost always greater than 0.7. In Finland, the scores show the worst results with a minimum MSESS around 0.3 for NGCD_rec-1 and around 0.4 for NGCD_rec-2. The observational network is denser over south Norway, where the MSESS can be close to 1 in some cases. The comparison between NGCD_rec-1 and NGCD_rec-2 in that region shows the similar differences pointed out above for the period 1971-2000.

The quality of the reconstruction depends on the season and it is proportional to the station density, as one can expect. Where the observational network is so dense that the CV-IDI is close to 1, the MSESS is also close to 1, and this happens for all the time periods considered, thus testifying the good quality of the RSOI method used in the reconstruction. Exceptions occur when there is presumably a significant difference between a station elevation and the average elevation of the points in the same area, as is discussed for NGCD_rec-1 over the western coast of Norway. From the insets in Figs. 5- 7 displaying MSESS versus CV-IDI, we can see that a sparser observational network, as the one used for 1901-2000, determines a faster decrease of the scores. However, they display a MSESS higher than 0.5 -on average- also for the period 1901-2000 and for data-sparse

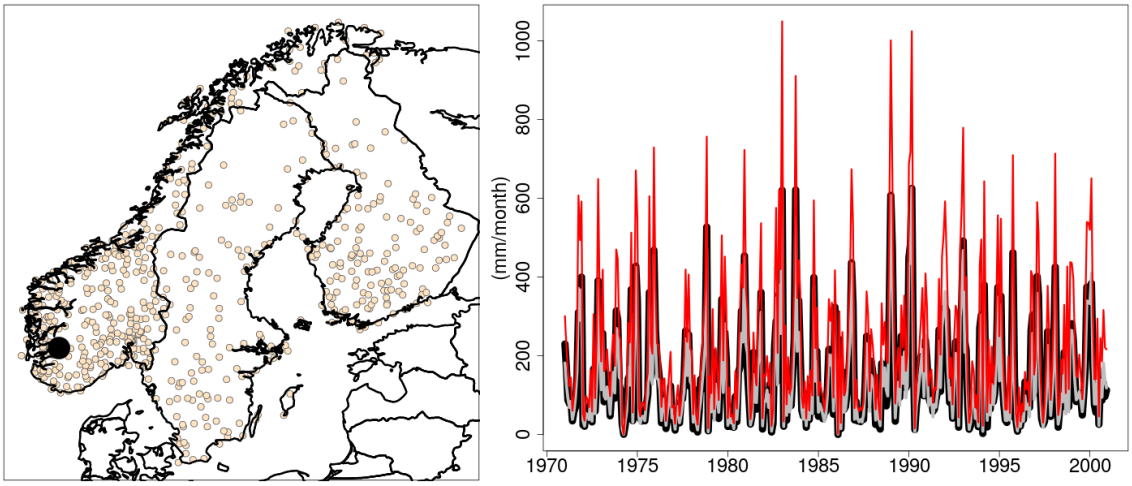

Figure 8: Time series of monthly precipitation amounts for a station in western Norway, which is marked with the black dot in the left panel. The time series are shown in the right panel for: station measurements (thick black line), NGCD_rec-1 1971-2000 (red line) and NGCD_rec-2 1971-2000 (gray line).

regions, that is where CV-IDI is less than 0.45.

5.2 Mean annual precipitation 1971-2000

The mean annual precipitation in the period 1971-2000 has been computed for NGCD and NGCD_rec, then they have been compared to assess the filtering properties of RSOI.

In Figure 10, the mean annual precipitation maps for NGCD_rec-1 1971-2000 and NGCD_rec-2 1971-2000 are shown. NGCD_rec-1 is based on NGCD-1, which takes into account the digital elevation model in the spatial analysis, therefore it is possible to recognize the details of the Scandinavian mountains in the corresponding figures. NGCD_rec-2 is based on NGCD-2, which is obtained without considering explicitly elevation in the interpolation. For both NGCD_rec datasets, the annual precipitation amount reaches its highest values along the Norwegian western coast, with some differences in the reconstructed amounts, especially at higher elevations. NGCD_rec-1 shows maximum values between 3000 mm and 4500 mm, while NGCD_rec-2 displays values between 3000 mm and 4000 mm. Those differences reflect the uncertainties in the estimation in a region that is a mesoscale hot spot of precipitation in Europe, where the observational network is rather dense but unevenly distributed along the range of altitudes as can be seen in Fig.1 of the paper by *Lussana et al.* (2019). Above the Arctic circle, in the inland region between Norway and Finland, the annual precipitation reaches its lowest values and in both

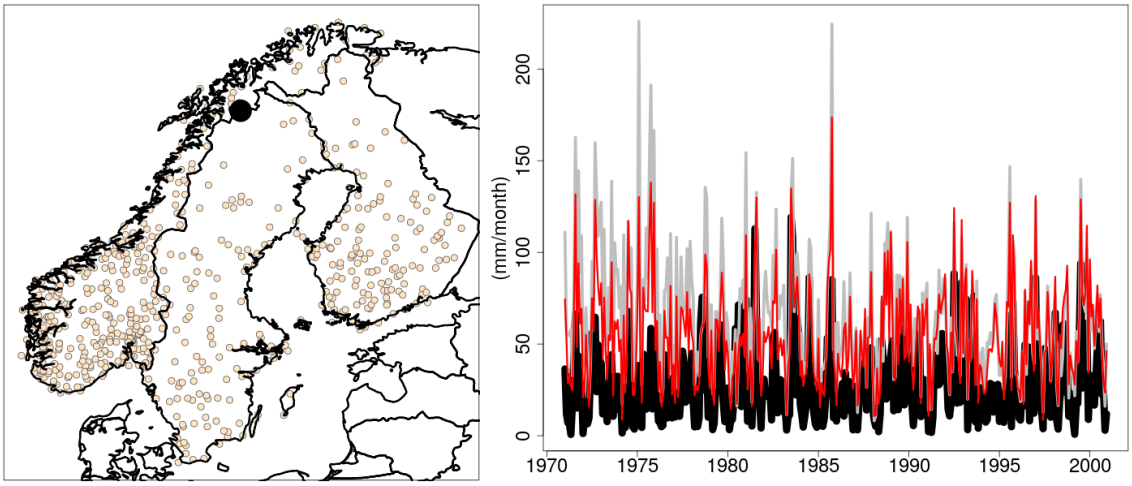

Figure 9: Time series of monthly precipitation amounts for a station on the range on the Scandinavian mountains close to the northernmost border between Norway and Sweden. The station is marked in the left panel with the black dot. The time series are shown in the right panel for: station measurements (thick black line), NGCD_rec-1 1971-2000 (red line) and NGCD_rec-2 1971-2000 (gray line).

datasets the annual precipitation is less than 500 mm.

Figure 11 shows the deviation between NGCD_rec 1971-2000 datasets and the corresponding NGCD datasets used for calibration in RSOI. Bluish colors indicate that NGCD_rec is wetter than NGCD, while brownish colors indicate that NGCD_rec is dryer than NGCD. The two maps in Fig. 11 show some similarities and some remarkable differences. The similarities are in the Lapland region (northern part of the domain) where both NGCD_rec-1/2 are wetter than their NGCD references, moreover, along the Norwegian coast NGCD_rec-1/2 are both dryer than the NGCD references. The most noticeable difference is in southern Sweden, where NGCD_rec-1 is significantly wetter than NGCD, while this is not the case for NGCD_rec-2. Analogously, in the easternmost part of Finland NGCD_rec-1 is dryer than NGCD-1, while this is not the case for NGCD_rec-2 when compared to NGCD-2.

The same comparison made in Figs. 10- 11 for NGCD_rec-1/2 1971-2000 has been made for NGCD_rec-1/2 1901-2000 in Figs. 12- 13. The time period considered for the comparison is again 1971-2000, since it is the period covered by NGCD. Despite the very different observational network used, Fig. 12 is remarkably similar to Fig. 10. The differences can be better appreciated in Fig. 13, where the anomalies are computed against the same NGCD reference datasets used in Fig. 11. NGCD_rec-1 1901-2000 smooths out the

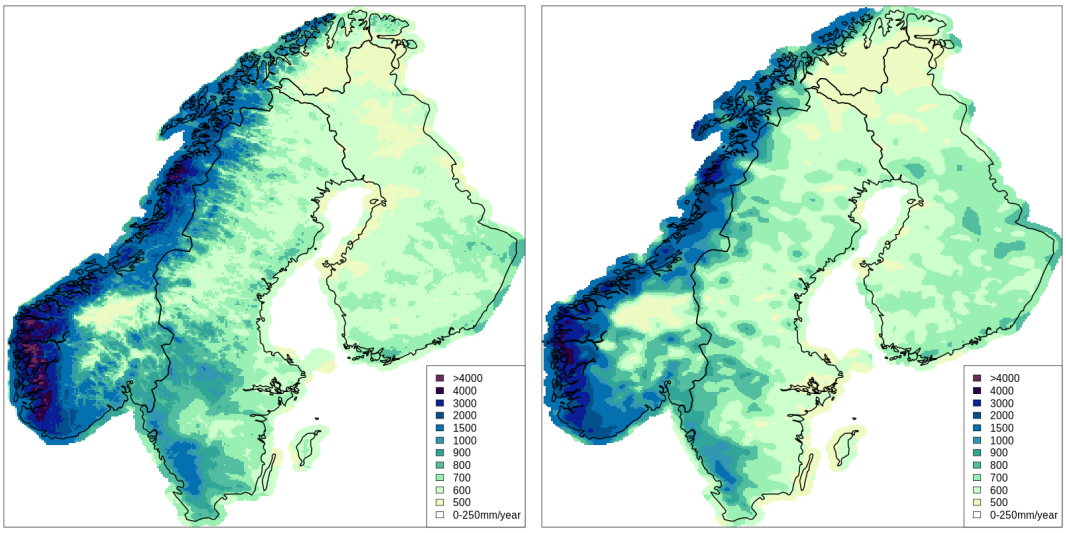

Figure 10: NGCD_rec mean annual total precipitation within the period 1971-2000. NGCD_rec-1 1971-2000 (left) and NGCD_rec-2 1971-2000 (right).

precipitation more than NGCD_rec-1 1971-2000, especially along the Norwegian coast. The same is true for NGCD_rec-2 1901-2000 compared against NGCD_rec-2 1971-2000, except for the coast of southern Norway, where NGCD_rec-2 1901-2000 is wetter than NGCD-2.

5.3 Temporal trends

The extraction of temporal trends of annual accumulated precipitation is presented as an example of application for NGCD_rec.

Trends are estimated using the Theil-Sen slope (*Sen*, 1968; *Theil*, 1992). The Mann-Kendall trend test (*Kendall*, 1975; *Mann*, 1945) is used to assess the statistical significance of each of the grid points, independently from the others. Then, the Benjamini-Hochberg meta test of the pertinent p-values (*Benjamini and Hochberg*, 1995) is used to adjust the assessment of the statistical significance based on multiple hypothesis testing theory, instead of considering independent tests.

The results are shown in Fig. 14 for NGCD_rec-1/2 1901-2000 as linear trends of precipitation per decade (mm/10-year). The statistical significance over domain is shown as the blue regions in the insets and the corresponding black contours on the maps. Bluish colors indicate an increase in precipitation, while brownish colors indicate a decrease in precipitation. There is a predominance of positive trends in precipitation and these trends are statistically significant. The only negative trends are in a mountainous region

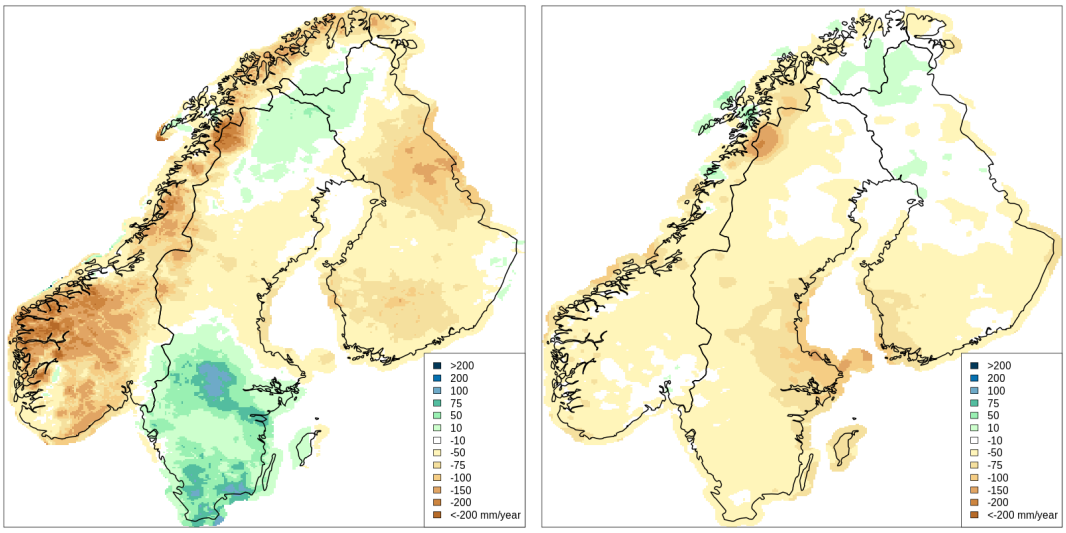

Figure 11: NGCD_rec mean annual total precipitation anomaly with respect to NGCD within the period 1971-2000. NGCD_rec-1 1971-2000 minus NGCD-1 1971-2000 (left) and NGCD_rec-2 1971-2000 minus NGCD-2 1971-2000 (right).

in northern Sweden, not too far from the Kebnekaise massif, which is the highest peak in Sweden at 2.120 m. This region is characterized by a sparse observational network, where the effect of a single station may explain the trend. It is worth noting that a positive trend between 10-20 mm/10-year is extracted from both datasets over Lapland, which is one of the driest places over the domain with an average annual precipitation 1971-2000 between 250mm and 500mm (see e.g. Fig. 12). The positive linear trend is greater along the western coast of Norway, where it reaches values up to 40-50 mm/10-year and where also the average precipitation amounts are the highest. Fig. 15 shows the time series of annual precipitation totals for the location along the coast of western Norway that is shown in the left panel of Fig. 8. The linear trends derived from NGCD_rec-1/2 1901-2000 are also shown and their values are: 46 mm/10-year for NGCD_rec-1 and 28 mm/10-year for NGCD_rec-2. As discussed in Sec. 5.1, this is a region characterized by complex terrain and the observational network struggles to provide a complete view of the events that occur there, therefore uncertainties in the reconstruction of the precipitation field must be expected. Thanks to the fact that NGCD_rec provides two different datasets, both plausible, we can get an idea of how this uncertainty impacts on the application in question.

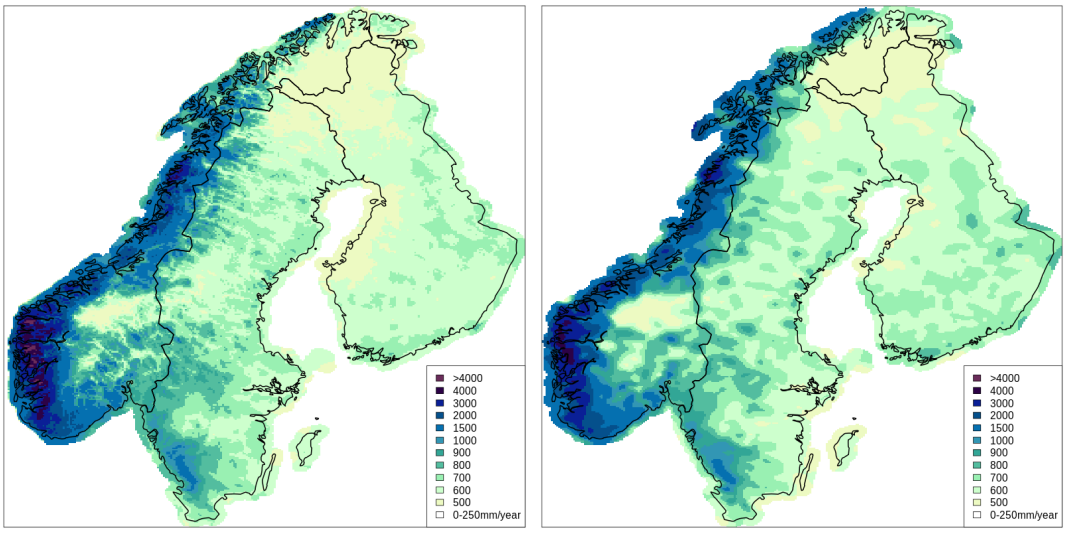

Figure 12: NGCD_rec mean annual total precipitation within the period 1901-2000. NGCD_rec-1 1901-2000 (left) and NGCD_rec-2 1901-2000 (right).

6 conclusions

NGCD_rec comes in two versions, NGCD_rec-1 and 2, depending on the spatial analysis method applied in the calibration of the RSOI method. NGCD_rec version 20.05 is a collection of 16 datasets and delivers observational gridded fields of monthly precipitation totals. The longest of those datasets cover the 100-year time period, from 1901 to 2000, and the use of available observations is optimized from ten years in ten years. In detail, the end of all time periods is always the year 2000, while the beginning of the period changes between datasets, with a timestep of 10 years, and each time we have used the most complete observational network available that is composed of continuous time series of monthly precipitation.

The calibration of NGCD_rec on the period 1971-2000 is based on the finer resolution dataset NGCD, which is available at a daily time scale and on a grid with a spacing of 1km. NGCD version 20.03 is obtained through well-established spatial interpolation methods and it makes use of all observations available in the data-richest period 1971-2000, regardless of whether the time series are continuous or not. NGCD is also made freely available for public download.

NGCD_rec version 20.05 covers Fennoscandia with a grid spacing of 5 km and it represents the first release of this dataset. The most important choice we made for the parameter settings is the number of principal components retained, which is fixed and set

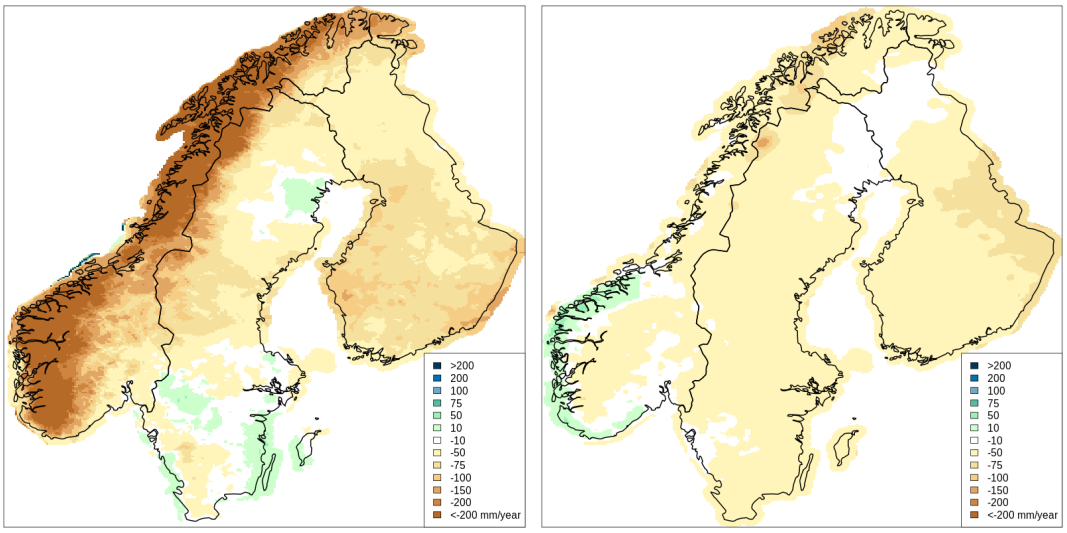

Figure 13: NGCD_rec mean annual total precipitation anomaly with respect to NGCD within the period 1901-2000. NGCD_rec-1 1901-2000 minus NGCD-1 1901-2000 (left) and NGCD_rec-2 1901-2000 minus NGCD-2 1971-2000 (right).

to 40 for all 16 datasets. A pre-processing step, before applying RSOI, is implemented and the data are transformed through Gaussian anamorphosis so as to reduce the skewness of their distribution.

We have presented results for NGCD_rec-1/2 1971-2000 based on 596 stations measuring continuously precipitation and we have compared them with NGCD_rec-1/2 1901-2000, which covers a 100-year period and it is based on a much sparser observational network of only 80 stations. These two time periods represent the extremes of the periods available in NGCD_rec with respect to the length of the reconstruction. The potential of RSOI in the reconstruction of gridded datasets is evident by comparing the mean annual precipitation maps obtained from NGCD_rec-1/2 1971-2000 and from NGCD_rec-1/2 1901-2000. In fact, the two maps look remarkably similar despite the dramatic differences in the respective observational networks.

The cross-validation summary statistics show that NGCD_rec-2 better predicts the observed values than NGCD_rec-1, especially in complex terrain. NGCD_rec-1 tries to compensate for the fact that the observations used come from stations with a representativeness error due to the fact that many of them are located on the valley floors and, therefore, NGCD_rec-1 shows higher precipitation values than the measured values. We believe that by making two datasets with different characteristics available simultaneously, we make it possible for users to evaluate the effect of uncertainty in the input

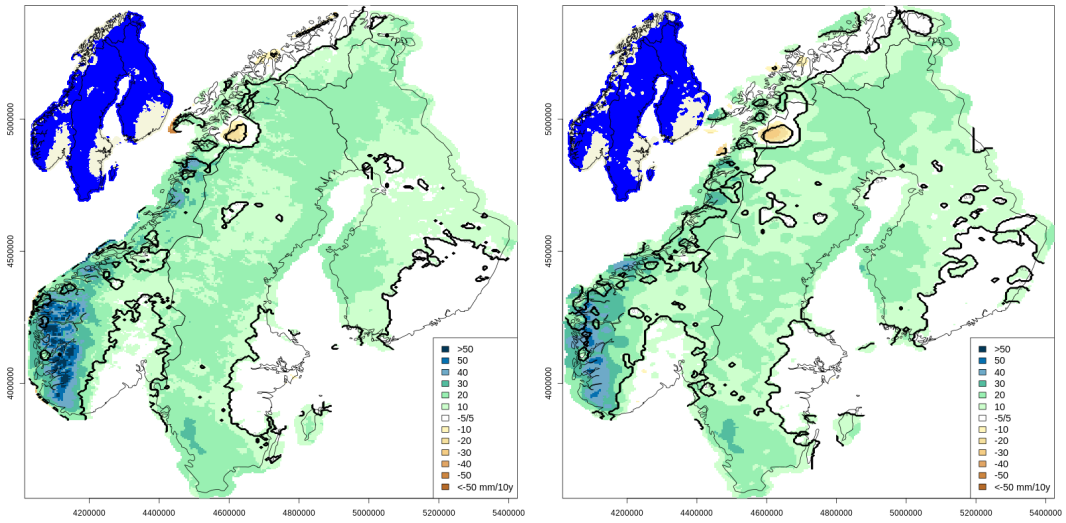

Figure 14: NGCD_rec decadal trends of annual total precipitation in the 100-year period 1901-2000. The color shades in the main maps shows the linear trends in mm/10years for NGCD_rec-1 1901-2000 (left) and NGCD_rec-2 1901-2000 (right). The insets at the top left corners show the areas where the trends are statistically significant in blue, the same areas are reported with black contours on the main maps. Statistical significance is assessed with the Mann-Kendall trend test, followed by a Benjamini-Hochberg meta-test with a critical false discovery rate of 0.05.

datasets on their applications (although in a limited fashion). From our evaluation over the period 1971-2000, we have verified that NGCD_rec-1 is more likely to overestimate precipitation by approximately 10% and the digital elevation model is clearly visible in the aggregated totals. The same evaluation shows that NGCD_rec-2 is more likely to underestimate precipitation by approximately 5% and the fields are smoother then those of NGCD_rec-1. The quality of the reconstructed fields depends on the seasonality of precipitation and on the local station density. In general, the NGCD_rec reconstructed fields are more in agreement with the observations in data-dense regions, nevertheless the quality of the fields does not decrease dramatically for data-sparse regions thanks to RSOI ability in using high-resolution information learned from the calibration period. When using NGCD_rec over Sweden and Finland for the first part of the twentieth century, from 1901 to 1950, one should always keep in mind that the amount of stations used is rather small and this will inevitably impact the quality of the results.

The extraction of linear trends is an important application of NGCD_rec and we have shown an example of application in this document. The temporal trends show a statisti-

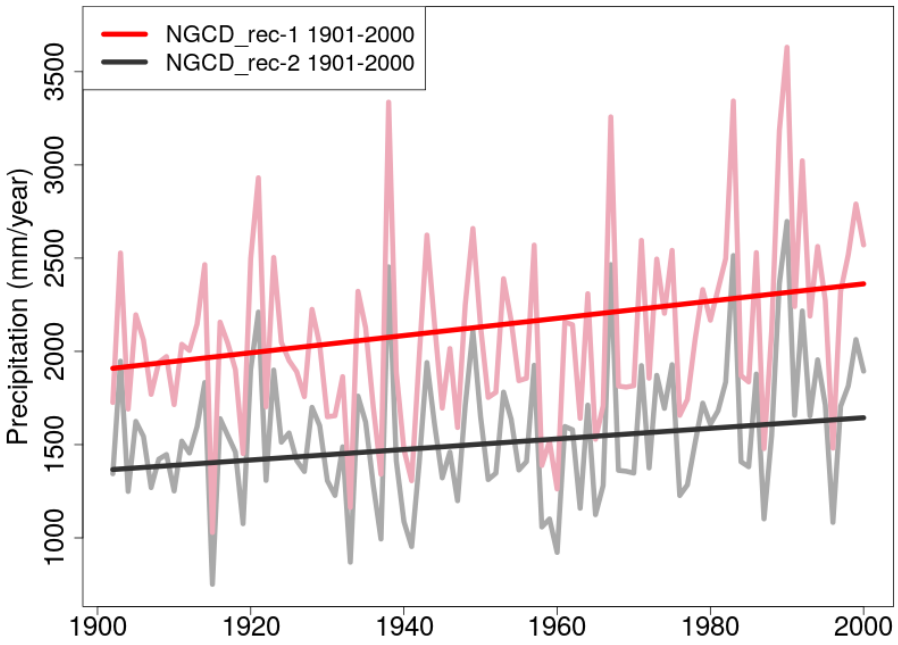

Figure 15: NGCD_rec-1/2 1901-2000 annual precipitation totals and linear trend extracted at the location in western Norway shown in Fig. 8.

cally significant increase in annual precipitation amounts during the period from 1901 to 2000 over large portions of Fennoscandia. The in-situ time series used have not been homogenized and the extracted trends are affected by possible inhomogeneities in the input data.

Regular updates of NGCD_rec are part of the future plans of MET Norway. In particular, we plan to update NGCD_rec once the ClimNorm initiative will make available a homogenized dataset of time series with monthly precipitation totals over the Nordic countries. Hopefully, this will also increase the number of available time series especially over Sweden and Finland in the period from 1901 to 1950.

A Data availability

NGCD_rec version 20.05 is freely available for public download at `https://thredds.met.no/thredds/catalog/ngcd/NGCD_rec_version_20.05/catalog.html`. The gridded data are stored in NetCDE files and they are complemented by metadata and descriptive attributes that have been included in the files. The coordinate reference system used is Lambert Azimuthal Equal Area (LAEA). The grid has a spacing of 5 km in both merid-

ional and zonal directions. In addition, latitude and longitude of the center of each grid box are provided as variables (lat and lon) within each file. NGCD version 20.03 is freely available for public download at `https://thredds.met.no/thredds/catalog/ngcd/version_20.03/catalog.html`.

B Acknowledgements

We acknowledge the data providers in the ECA&D project. Data and metadata available at `https://www.ecad.eu`. The European Centre for Medium-Range Weather Forecasts (ECMWF) implements the Copernicus Climate Change Service on behalf of the European Union, and NGCD_rec was produced with funding from this Service.

We would like to thank Christoph Frei for providing the gridrsoi Package and for his patient, unfailing support during the course of this work.

References

Benjamini, Y., and Y. Hochberg (1995), Controlling the false discovery rate: A practical and powerful approach to multiple testing, *Journal of the Royal Statistical Society. Series B (Methodological)*, *57*(1), 289–300.

Cardinali, C., S. Pezzulli, and E. Andersson (2004), Influence-matrix diagnostic of a data assimilation system, *Quarterly Journal of the Royal Meteorological Society*, *130*(603), 2767–2786, doi:10.1256/qj.03.205.

Carrassi, A., M. Bocquet, L. Bertino, and G. Evensen (2018), Data assimilation in the geosciences: an overview of methods, issues, and perspectives, *Wiley Interdisciplinary Reviews: Climate Change*, *9*(5), e535, doi:10.1002/wcc.535.

Cornes, R. C., G. van der Schrier, E. J. M. van den Besselaar, and P. D. Jones (2018), An ensemble version of the E-OBS temperature and precipitation data sets, *Journal of Geophysical Research: Atmospheres*, *123*(17), 9391–9409, doi:10.1029/2017JD028200.

Gandin, L. S., and R. Hardin (1965), *Objective analysis of meteorological fields*, vol. 242, Israel program for scientific translations Jerusalem.

Gesch, D. B., K. L. Verdin, and S. K. Greenlee (1999), New land surface digital elevation model covers the earth, *Eos, Transactions American Geophysical Union*, *80*(6), 69–70, doi:https://doi.org/10.1029/99EO00050.

Gisnås, K., B. Etzelmüller, C. Lussana, J. Hjort, A. B. K. Sannel, K. Isaksen, S. Westermann, P. Kuhry, H. H. Christiansen, A. Frampton, et al. (2016), Permafrost map for Norway, Sweden and Finland, *Permafrost and Periglacial Processes*.

Golding, B. W. (1998), Nimrod: a system for generating automated very short range forecasts, *Meteorological Applications*, *5*(1), 1–16, doi:https://doi.org/10.1017/S1350482798000577.

Hager, W. W. (1989), Updating the inverse of a matrix, *SIAM Review*, *31*(2), 221–239, doi:10.1137/1031049.

Hisdal, H., and O. E. Tveito (1993), Extension of runoff series using empirical orthogonal functions, *Hydrological Sciences Journal*, *38*(1), 33–49, doi:10.1080/02626669309492638.

Isotta, F. A., M. Begert, and C. Frei (2019), Long-term consistent monthly temperature and precipitation grid data sets for switzerland over the past 150 years, *Journal of Geophysical Research: Atmospheres*, *124*(7), 3783–3799, doi:10.1029/2018JD029910.

Jazwinski, A. H. (2007), *Stochastic processes and filtering theory*, Courier Dover Publications.

Kendall, M. G. (1975), *Rank correlation methods*, Griffin, London.

Klein Tank, A., J. Wijngaard, G. Können, R. Böhm, G. Demarée, A. Gocheva, M. Mileta, S. Pashiardis, L. Hejkrlik, C. Kern-Hansen, et al. (2002), Daily dataset of 20th-century surface air temperature and precipitation series for the European climate assessment, *International journal of climatology*, *22*(12), 1441–1453.

Lussana, C., T. Saloranta, T. Skaugen, J. Magnusson, O. E. Tveito, and J. Andersen (2018a), seNorge2 daily precipitation, an observational gridded dataset over Norway from 1957 to the present day, *Earth System Science Data*, *10*(1), 235–249, doi:10.5194/essd-10-235-2018.

Lussana, C., O. E. Tveito, and F. Uboldi (2018b), Three-dimensional spatial interpolation of 2m temperature over Norway, *Quarterly Journal of the Royal Meteorological Society*, *144*(711), 344–364, doi:10.1002/qj.3208.

Lussana, C., O. E. Tveito, A. Dobler, and K. Tunheim (2019), senorge_2018, daily precipitation, and temperature datasets over norway, *Earth System Science Data*, *11*(4), 1531–1551, doi:10.5194/essd-11-1531-2019.

Lussana, C., T. N. Nipen, I. A. Seierstad, and C. A. Elo (2021), Ensemble-based statistical interpolation with gaussian anamorphosis for the spatial analysis of precipitation, *Nonlinear Processes in Geophysics*, *28*(1), 61–91, doi:10.5194/npg-28-61-2021.

Mann, H. B. (1945), Nonparametric tests against trend, *Econometrica*, *13*(3), 245–259.

Mohr, M. (2008), New routines for gridding of temperature and precipitation observations for "senorge. no", *Met. no Report*, *8*, 2008.

Mohr, M. (2009), Comparison of versions 1.1 and 1.0 of gridded temperature and precipitation data for Norway, *Norwegian Meteorological Institute, met no note*, *19*.

Nipen, T. N., I. A. Seierstad, C. Lussana, J. Kristiansen, and Ø. Hov (2020), Adopting citizen observations in operational weather prediction, *Bulletin of the American Meteorological Society*, *101*(1), E43–E57, doi:10.1175/BAMS-D-18-0237.1.

Saloranta, T. (2012), Simulating snow maps for Norway: description and statistical evaluation of the seNorge snow model, *The Cryosphere*, *6*(6), 1323–1337.

Saloranta, T. M. (2016), Operational snow mapping with simplified data assimilation using the senorge snow model, *Journal of Hydrology*, *538*, 314–325.

Schiemann, R., M. A. Liniger, and C. Frei (2010), Reduced space optimal interpolation of daily rain gauge precipitation in switzerland, *Journal of Geophysical Research: Atmospheres*, *115*(D14), n/a–n/a, doi:10.1029/2009JD013047.

Sen, P. K. (1968), Estimates of the regression coefficient based on kendall's tau, *Journal of the American Statistical Association*, *63*(324), 1379–1389, doi:10.1080/01621459.1968.10480934.

Skaugen, T., and Z. Mengistu (2016), Estimating catchment-scale groundwater dynamics from recession analysis-enhanced constraining of hydrological models, *Hydrology and Earth System Sciences*, *20*(12), 4963.

Skaugen, T., and C. Onof (2014), A rainfall-runoff model parameterized from gis and runoff data, *Hydrological Processes*, *28*(15), 4529–4542.

Tarantola, A. (2005), *Inverse Problem Theory and methods for model parameter estimation*, SIAM, Philadelphia.

Theil, H. (1992), A rank- invariant method of linear and polynomial regression analysis, *Proceedings of the Royal Netherlands Academy of Sciences*, *53*, 386-392, doi:https://doi.org/10.1007/978-94-011-2546-8_20.

Tveito, O. E., and H. Hisdal (1994), A study of regional trends in annual and seasonal precipitation and runoff series, *Tech. Rep. 09*, Norwegian Water Resources and Energy Directorate.

Tveito, O. E., I. Bjørdal, A. O. Skjelvåg, and B. Aune (2005), A gis-based agro-ecological decision system based on gridded climatology, *Meteorological Applications*, *12*(1), 57–68.

Tveito, O. E., S. Aniskeviča, J. Cappelen, E. Engström, H. M. Gjelten, C. D. Jensen, P. Jokinen, E. K. Kuya, C. Lussana, A. Mäkelä, K. Mändla, K. Vint, L. Wern, and V. Zandersons (2020), Climnorm - temperature data set, gap filling methods and regional analysis to prepare new climate normals, *Tech. Rep. 04*, Norwegian Meteorological Institute.

Uboldi, F., and A. Buzzi (1994), Successive-correction methods applied to mesoscale meteorological analysis, *Il Nuovo Cimento C*, *17*(6), 745–761.

Uboldi, F., C. Lussana, and M. Salvati (2008), Three-dimensional spatial interpolation of surface meteorological observations from high-resolution local networks, *Meteorological Applications*, *15*(3), 331–345.

Wilks, D. S. (2019), *Statistical methods in the atmospheric sciences (Fourth Edition)*, fourth edition ed., Elsevier, doi:https://doi.org/10.1016/B978-0-12-815823-4.00009-2.

Table 1: Summary of the available NGCD_rec datasets and the number of complete stations used in the reconstruction. N "global" is the total number of stations. N "data-sparse" is the number of stations in data-sparse regions. N "data-dense" is the number of stations in data-dense regions. D is the median of the distances between a station and its closest third station.

dataset label	N global	N data-sparse	N data-dense	D (km)
NGCD_rec-1/2 1971-2000	596	7	540	37
NGCD_rec-1/2 1961-2000	373	8	300	43
NGCD_rec-1/2 1951-2000	294	11	218	50
NGCD_rec-1/2 1941-2000	224	19	162	53
NGCD_rec-1/2 1931-2000	201	19	136	57
NGCD_rec-1/2 1921-2000	145	24	93	56
NGCD_rec-1/2 1911-2000	117	26	66	62
NGCD_rec-1/2 1901-2000	80	20	39	73

Table 2: Summary of NGCD_rec MSESS statistics for each season. The MSESS is reported as a triples of values $x\,(y,z)$, where: x is the mean over all stations, y and z are the means over stations in data-sparse and data-dense regions, respectively. The data-sparse and -dense regions are defined as in Tab. 1.

	MSESS			
dataset label	spring	summer	autumn	winter
NGCD_rec-1 1971-2000	0.77 (0.79,0.79)	0.71 (0.78,0.72)	0.77 (0.82,0.79)	0.79 (0.83,0.81)
NGCD_rec-1 1961-2000	0.77 (0.65,0.80)	0.69 (0.53,0.70)	0.75 (0.62,0.78)	0.79 (0.61,0.81)
NGCD_rec-1 1951-2000	0.74 (0.37,0.78)	0.66 (0.52,0.68)	0.74 (0.61,0.76)	0.76 (0.57,0.79)
NGCD_rec-1 1941-2000	0.76 (0.59,0.80)	0.65 (0.54,0.68)	0.74 (0.66,0.76)	0.77 (0.64,0.80)
NGCD_rec-1 1931-2000	0.75 (0.53,0.80)	0.63 (0.51,0.67)	0.74 (0.64,0.77)	0.75 (0.57,0.80)
NGCD_rec-1 1921-2000	0.75 (0.57,0.82)	0.65 (0.54,0.68)	0.75 (0.64,0.78)	0.76 (0.62,0.81)
NGCD_rec-1 1911-2000	0.76 (0.59,0.83)	0.66 (0.53,0.71)	0.76 (0.65,0.80)	0.77 (0.62,0.83)
NGCD_rec-1 1901-2000	0.73 (0.54,0.82)	0.65 (0.47,0.72)	0.75 (0.62,0.80)	0.74 (0.57,0.81)
NGCD_rec-2 1971-2000	0.82 (0.75,0.84)	0.79 (0.75,0.80)	0.84 (0.80,0.87)	0.86 (0.82,0.89)
NGCD_rec-2 1961-2000	0.79 (0.64,0.85)	0.75 (0.54,0.78)	0.78 (0.67,0.86)	0.83 (0.68,0.88)
NGCD_rec-2 1951-2000	0.80 (0.50,0.84)	0.74 (0.54,0.78)	0.82 (0.63,0.85)	0.83 (0.64,0.87)
NGCD_rec-2 1941-2000	0.81 (0.61,0.86)	0.74 (0.54,0.79)	0.83 (0.67,0.86)	0.84 (0.66,0.88)
NGCD_rec-2 1931-2000	0.80 (0.57,0.86)	0.72 (0.52,0.78)	0.82 (0.66,0.86)	0.82 (0.61,0.87)
NGCD_rec-2 1921-2000	0.80 (0.60,0.87)	0.72 (0.55,0.79)	0.82 (0.67,0.88)	0.82 (0.64,0.89)
NGCD_rec-2 1911-2000	0.79 (0.61,0.88)	0.71 (0.53,0.80)	0.82 (0.67,0.89)	0.81 (0.63,0.90)
NGCD_rec-2 1901-2000	0.77 (0.54,0.88)	0.70 (0.48,0.82)	0.80 (0.63,0.90)	0.79 (0.57,0.90)